Colloids and Surfaces A: Physicochem. Eng. Aspects 408 (2012) 114–121

Contents lists available at SciVerse ScienceDirect

Colloids and Surfaces A: Physicochemical and Engineering Aspects

journal homepage: www.elsevier.com/locate/colsurfa

Influence of morphology and surface exchange reaction on magnetic properties of monodisperse magnetite nanoparticles

Mengjie Song[a], Yu Zhang[a,*], Sunling Hu[a], Lina Song[a], Jinlai Dong[a], Zhongping Chen[b], Ning Gu[a]

[a] State Key Laboratory of Bioelectronics, Jiangsu Key Laboratory for Biomaterials and Devices, School of Biological Science and Medical Engineering, Southeast University, Nanjing 210096, PR China
[b] Institute for Nautical Medicine, Nantong University, Nantong 226001, PR China

HIGHLIGHTS

- Magnetic Fe_3O_4 NPs with different shape but the same size and surface were obtained.
- Samples were monodisperse which hardly changed using longer ligand exchange time.
- Magnetism was compared based on different morphology and ligand exchange time.
- Sample surfaces were destroyed during ligand exchange, leaving magnetism weakened.
- Quasi-cubical sample had better magnetism than spherical one under comparable condition

GRAPHICAL ABSTRACT

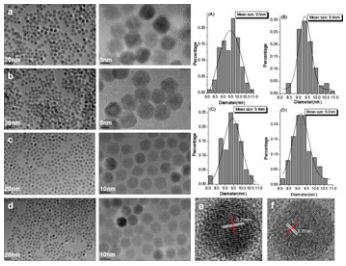

ARTICLE INFO

Article history:
Received 26 November 2011
Received in revised form 23 May 2012
Accepted 28 May 2012
Available online 5 June 2012

Keywords:
Monodisperse Fe_3O_4 NPs
Morphology
Surface ligand exchange
Magnetism

ABSTRACT

Monodisperse magnetite nanoparticles (Fe_3O_4 NPs) were synthesized by thermal decomposition of Fe(oleate)$_3$ in 1-octadecene containing oleic acid. Two kinds of oleic acid capped Fe_3O_4 nanoparticles (Fe_3O_4@OA) with different shape but similar size were obtained, quasi-cubical and spherical respectively. Ligand exchange reaction with 2,3-dimercaptosuccinic acid (DMSA) was performed to transfer Fe_3O_4 NPs from organic phase to aqueous phase. TEM, DLS and EDS were used to characterize and evaluate these samples. TEM showed that ligand exchange reaction made the nanoparticles shape changed, especially the quasi-cubical ones. With EDS analysis, effects of surface exchange on Fe_3O_4@DMSA NPs were further studied. Magnetic properties, including saturation magnetization (M_s), relaxivity (r_2) of Fe_3O_4 NPs as MRI contrast agent and specific absorption rate (SAR) in alternating magnetic field, were investigated with respect to Fe_3O_4 nanoparticle morphology and surface exchange time. Results showed that nanoparticles of quasi-cubical shape, obtained using shorter surface exchange time, had stronger saturation magnetization which accordingly resulted in better MRI contrast and heat conversion efficiency under magnetic induction.

1. Introduction

Magnetic nanoparticles, as an important branch of nanomaterials, are bringing more and more exciting improvements for various fields [1–7], especially biomedical engineering. For instance, magnetic nanoparticles as negative contrast agents for MR imaging were extensively investigated [8,9]. Utilizing their heat effect under

* Corresponding author. Tel.: +86 25 83792576; fax: +86 25 8379496.
E-mail addresses: zhangyu@seu.edu.cn (Y. Zhang), guning@seu.edu.cn (N. Gu).

0927-7757/$ – see front matter © 2012 Elsevier B.V. All rights reserved.
http://dx.doi.org/10.1016/j.colsurfa.2012.05.039

alternating magnetic field (AMF), magnetic nanoparticles can be used in cancerous hyperthermia [10]. Delivery of drug or gene to the specific targets is also achievable with magnetic nanoparticles. Of abundant magnetic nanomaterials [11–16], magnetic iron oxide nanoparticles (usually Fe_3O_4 and Fe_2O_3) are exclusively widely studied not only due to their excellent magnetic response but also their low toxicity and bio-safety, for Fe is one trace element essential for our body, and extra Fe ion in cytoplasm can be regulated by ferritin and transferrin receptor [16]. In light of these recognized advantages, studies about iron oxide nanoparticles have prevailed since last decades and many achievements have been received.

As we all know, materials' applications rely on their properties, while their properties are determined by many aspects of themselves, such as size and its distribution, surface coating, aggregation state, shape, and so on. This dependence is especially highlighted for nanoparticles due to their finite size. The effects of nanoparticle size and surface on physical and chemical properties have been extensively investigated [17–19]. For example, through size control, the magnetization behavior, MRI contrast enhancement efficacy and magnetically induced heating effect can be modulated significantly and the optimal size for different applications has been suggested [20–22]. For accurate comparison, the nanoparticles are required to be monodisperse in size so that each individual nanoparticle has nearly identical physical and chemical properties. Using size-sorted anionic maghemite nanoparticles with sizes from 5 to 16.5 nm, SAR values were varied by 3 orders of magnitude with increasing particle size (from 4 to 1650 w/g at 700 kHz and 24.8 kA/m) [22]. With monodisperse spherical MEIO (magnetism-engineered iron oxide) nanoparticles, Lee et al. [15] certified the MR signals enhance remarkably with increasing size in the range of 6–12 nm. Surface coating affects the magnetization of nanoparticles through modifying surface spin disorders and also modulates MRI relaxivity of nanoparticles by altering the diffusion of water molecules between the solution phase and the adjacent layer surrounding the particle surface [23]. In addition to size and surface chemistry, aggregation state also considerably contributes to magnetic properties of nanoparticles, which has been demonstrated widely [24]. For instance, Roca et al. [25] discovered that proper aggregation was advantageous for MRI enhancement.

As magnetic nanoparticles with different sizes and surfaces have different aggregation state in solution due to the size dependence of magnetic dipole interaction and colloidal stability relying on surface molecule modification, we should be particularly careful when exploring the size and surface dependence of magnetic properties. Similarly, to investigate shape effects, nanoparticles involved should be of same size distribution, surface coating and aggregation state or at least approximately. This is very difficult so that much fewer reports concern accurate investigation about shape effect, though nanoparticles with various shapes (such as spherical, cubical, bipyramidal, octahedral and so on) have been synthesized. Recently, Salazar–Alvarez et al. [26] reported that different surface and magnetocrystalline anisotropy resulted in different blocking temperature of T_B for monodispersive spherical and cubical γ-Fe_2O_3 nanoparticles with the same oleate coating and similar size (14.5 ± 0.8 nm for spherical diameter and 12 ± 2.5 nm for cubic edge length). However, for biomedical applications, one prefers water-soluble magnetic nanoparticles rather than organic soluble nanoparticles. Here, we investigate water-soluble Fe_3O_4 nanoparticles obtained by surface exchange of oleate with DMSA, and these monodispersive nanoparticles have different shape (quasi-cubical and spherical) and more approximate size (9.5 nm and 9.6 nm). The oleate coated Fe_3O_4 NPs were synthesized by a well-established thermal decomposition method [27–31] using iron oleate as precursor in a high boiling solvent of 1-octadecene containing oleic acid, and the shape was accurately controlled by variation of both reaction time and amount of oleic acid. We also found the surface exchange could modify the morphology, and accordingly alter their magnetic properties. Therefore, the direct investigate of water-soluble Fe_3O_4 nanoparticles is more significant for guiding biomedical applications. In this aspect, saturation magnetization (M_s), MRI (magnetic resonance imaging) relaxivity (r_2), specific absorption rate (SAR) value were investigated because they are three important parameters representing the capacity of superparamagnetic nanoparticles in magnetic mediated separation or targeting, MRI contrast enhancement, and heat conversion in cancerous hyperthermia, respectively.

2. Experiment

2.1. Materials

Sodium oleate, ferric trichloride hexahydrate ($FeCl_3 \cdot 6H_2O$), acetone, hexane, ethanol, trithylamine, 2,3-dimercaptosuccinic acid (DMSA), anhydrous sodium acetate (NaAc), acetic acid (HAc) were purchased from Sinopharm Chemical Reagent Co. Ltd. China. Oleic acid of chemical pure was purchased from Shanghai Lingfeng Chemical Reagent Co. Ltd. China. 1-Octadecene was purchased from Alfa Aesar. All reagents were used without any further treatment. Deionized water was produced by Aquapro water purification machine (EDI1-1001-U, Yiyang, China).

2.2. Synthesis of Fe_3O_4 nanoparticles

2.2.1. Preparation of Oleic acid coated magnetite nanoparticles (Fe_3O_4@OA NPs)

Fe_3O_4 NPs were synthesized by pyrolysis of Fe-oleate complex in high boiling point solvent, 1-octadecene. In advance, $Fe(oleate)_3$ was prepared as the precursor following a reported procedure [30,31]. 4 mmol as-prepared $Fe(oleate)_3$ was mixed with 0.7 ml oleic acid and 20 ml 1-octadecene under ultrasonication and vigorous stirring. The mixture was put into a 50 ml three-neck flask, and heated from room temperature to 110 °C. Keeping 110 °C for half an hour, the moisture produced was excluded. The reaction was continuously heated up from 110 °C to 320 °C (3.5 °C/min) in one hour, which is favorable for the formation of monodisperse nanoparticles. After 20 min refluxing at 320 °C, the black fluid was transferred to a beaker and washed with ethanol for three times. To remove residual 1-octadecene in the final system, the black fluid was again washed with hexane/acetone for three cycles. The black precipitate at the bottom of the beaker was dissolved in hexane. This sample was named as o-sample-1.

Changing the amount of surfactant and the refluxing time, we synthesized o-sample-2: 0.6 ml oleic acid was used and the refluxing time was shortened to 5 min.

2.2.2. Preparation of DMSA coated magnetite nanoparticles (Fe_3O_4@DMSA NPs)

Samples above were only oil-soluble and not suitable for direct biomedical applications. Ligand exchange with 2,3-dimercaptosuccinic acid (DMSA) molecules was carried out to make samples hydrophilic and usable. Two samples obtained in last experiment were dried in vacuum oven for 48 hours in advance. 300 mg dried sample dispersed in 100 ml hexane and 150 mg DMSA dispersed in 100 ml acetone as well as 150 μl triethylamine were added into a 500 ml three-neck flask one after another. After 4 h mechanical stirring and refluxing, black precipitate appeared at the bottom, demonstrating DMSA molecules had been conjugated onto the surface of Fe_3O_4 NPs. A homogeneous colloid was obtained by dissolving it with deionized water. After further purification by dialysis (MW cutoff of 14 kDa) against deinoized water (pH 7) for 1 day, the resultant solution was stored at 4 °C.

It has been verified that fully ligand exchange would destroy the surface of nanoparticles [32,33], with their size decreased or shape defected. Here, adjusting the ligand exchange time to 30 min, another two Fe_3O_4@DMSA samples were prepared. So far, four hydrophilic samples were obtained, which were the very targets we took to study the correlation between shape and property. For o-sample-1, samples acquired after 30 min and 4 h reaction were named as quasi-cubical-30 min and quasi-cubical-4 h, respectively. Similarly, spherical-30 min and spherical-4 h represented samples stemmed from o-sample-2.

2.3. Fe content determination

Fe content of each Fe_3O_4@DMSA sample was determined with a C–A (absorbance versus iron concentration, $r = 0.99998$) calibration curve, which was established with 1,10-phenanthroline spectrophotometric method [34] on UV–visible spectrophotometer (UV-3600, SHIMADZU, Japan). 50 μl Fe_3O_4@DMSA sample in a 50 ml volumetric flask was dissociated by 2 ml hydrochloric acid (HCl, 6 M). After sonication for 20 min, 1 ml 10% hydroxylamine hydrochloride was added to reduce Fe^{3+} to Fe^{2+}. So far, all Fe elements existed in the form of Fe^{2+}. After 5 ml sodium acetate buffer (pH 5.0) addition, the whole system turned reddish orange due to the formation of Fe^{2+}-1,10-phenanthroline compound. After standing at room temperature for 20 min, it was diluted to 50 ml with deionized water. The absorbance at 510 nm (the maximum absorbance wavelength of Fe^{2+}-1,10-phenanthroline compound) was measured. Referring the calibration curve, iron concentration was given automatically with UV–visible spectrophotometer.

2.4. Characterization

The core size and morphology of two Fe_3O_4@OA and four Fe_3O_4@DMSA samples were characterized with a transmission electron microscopy (TEM, JEOL, Tokyo, Japan) operating at 120.0 kV. High resolution TEM (HRTEM) images of two 30 min ligand-exchanged Fe_3O_4@DMSA samples were obtained, which would further determine their crystalline structure. Hydrodynamic diameters of four Fe_3O_4@DMSA samples were measured with a particle size analyzer (Malvern Zetasizer, UK). Energy dispersive spectrum was characterized on X-ray energy dispersive spectrometer (SEM–EDS, S-3400 N II, Hitachi, Japan). Vibrating sample magnetometer (VSM, Lakeshore VSM 7407, USA) was utilized to characterize their magnetism.

2.5. MRI experiment

MRI experiment was carried out on a clinical 1.5 T MR scanner (Avanto, Siemens, Germany). T_2 relaxation times were determined with a multi-echo spin-echo sequence (16 echoes; repetition time (TR) = 2500 ms; echo time (TE) = 22–352 ms). For each sample, T_2-weighted images of ten different Fe concentration samples (0, 0.625, 1.00, 1.25, 2.00, 2.50, 4.00, 5.00, 8.00, 10.0 μg/ml) were got. The relaxation time T_2 was obtained by calculating the signal intensity in 0.3 cm^2 region of interest on each image. The relaxivity (r_2) was just the slope of R_2–C ($R_2 = 1/T_2$, C is Fe concentration) curve.

2.6. Heating effect measurement

Due to Brownian relaxation and Neel relaxation losses, superparamagnetic nanoparticles under alternating magnetic field (AMF) can generate heat, which has been widely studied and utilized in magnetic mediated hyperthermia. SAR (specific absorption rate) describing the heat generated per time and mass and is always taken as the main indicator. This experiment was preformed on an alternating magnetic field, in which, the frequency and amplitude were 100 kHz and 30.0 kA/m, respectively. When tested, the samples of uniform concentration (0.6 mg Fe/ml) were put into a magnetic induction coil with a diameter of about 5 cm. The temperature variation along with time was recorded with an optical fiber probe inserted into the tested sample solutions. SAR was calculated with the following equation [35]:

$$\mathrm{SAR} = C \cdot \frac{\Delta T}{\Delta t} \cdot \frac{1}{m_{\mathrm{Fe}}} \quad (1)$$

where C is the specific heat capacity of the sample; $\Delta T/\Delta t$ is the initial slope of the curve of temperature change versus time; m_{Fe} is the Fe content in one gram Fe_3O_4 NPs solution.

3. Results and discussions

In the thermal decomposition, iron precursor, surfactant, solvent, reaction temperature and time are the main factors influencing the final morphology and structure of as-synthesized nanoparticles. Here we changed the surfactant amount and the refluxing time to control particles size and shape. Fig. 1 illustrated their respective TEM images and size distributions. As the results shown, o-sample-1 and o-sample-2 were highly monodisperse, with similar size but different shape, quasi-cubical (Fig. 1a, $d = 9.5$ nm) and spherical (Fig. 1b, $d = 9.6$ nm), respectively. The preparation details elaborated in the experimental section indicated that more oleic acid and longer reaction time eventually generated quasi-cubical nanoparticles. Similar synthetic strategy has been also reported currently by Campbell et al. to prepare the quasi-cubical magnetite nanoparticles, and a large scale synthesis of such nanoparticles was achieved (at least up to 10 g particles per batch) [36]. In their synthesis, for comparison, a similar feeding amount of oleic acid but a longer reaction time of 30 min at 320 °C was employed and thus resulted in a larger nanoparticle size. Referring to the mechanism of nanoparticles fabrication, monomer, nucleation and further growth of the nuclei are commonly considered as the three key steps. Throughout this process, monomer plays an important role. In the classical LaMer principle [37], nanoparticles form and further grow only when the monomer concentration supersaturated at which it can overcome an energy barrier. At the initial phase of growth, nanoparticles yielded were nearly spherical due to the thermodynamically controlled lowest energy principle. As the growth proceeded, monomer were consumed, and growth along with the ⟨1 1 1⟩ facet of higher surface energy was preferred [38,39], and thus the nanoparticles shape turned to cubical. Also, the surfactant is important. As we all know, the surfactants act as a protective layer on the metastable inorganic nanoparticles, and enough surfactants are desired to ensure every nanoparticles are well chelated and stable. When lacking of surfactants, the nanoparticles will be of wide size distribution and poor uniformity. Here, more oleic acid was used to complement the volatilized oleic acid during the prolonged reaction time. Besides, maybe the more oleic acid also played a facet-selective growth, which had been proposed by Maksym [40].

For biomedical applications, the nanoparticles are necessarily biocompatible, at least hydrophilic. Ligand exchange with DMSA was performed for all four samples. Through ligand exchange, the pre-existing hydrophobic oleic acid molecules on the surface of Fe_3O_4 NPs were replaced by hydrophilic DMSA ligands, making the nanoparticles water dispersible. It was demonstrated that, with FTIR analysis, DMSA molecules were conjugated chemically on the surface of Fe_3O_4 nanoparticles according to the characteristic peaks of symmetric and asymmetric COO^- stretching vibration of DMSA, as previously reported [31]. The S—S bonds formation by oxidation of —SH groups during the exchange reaction were also confirmed by Raman spectroscopy, which increased the conjugating amount

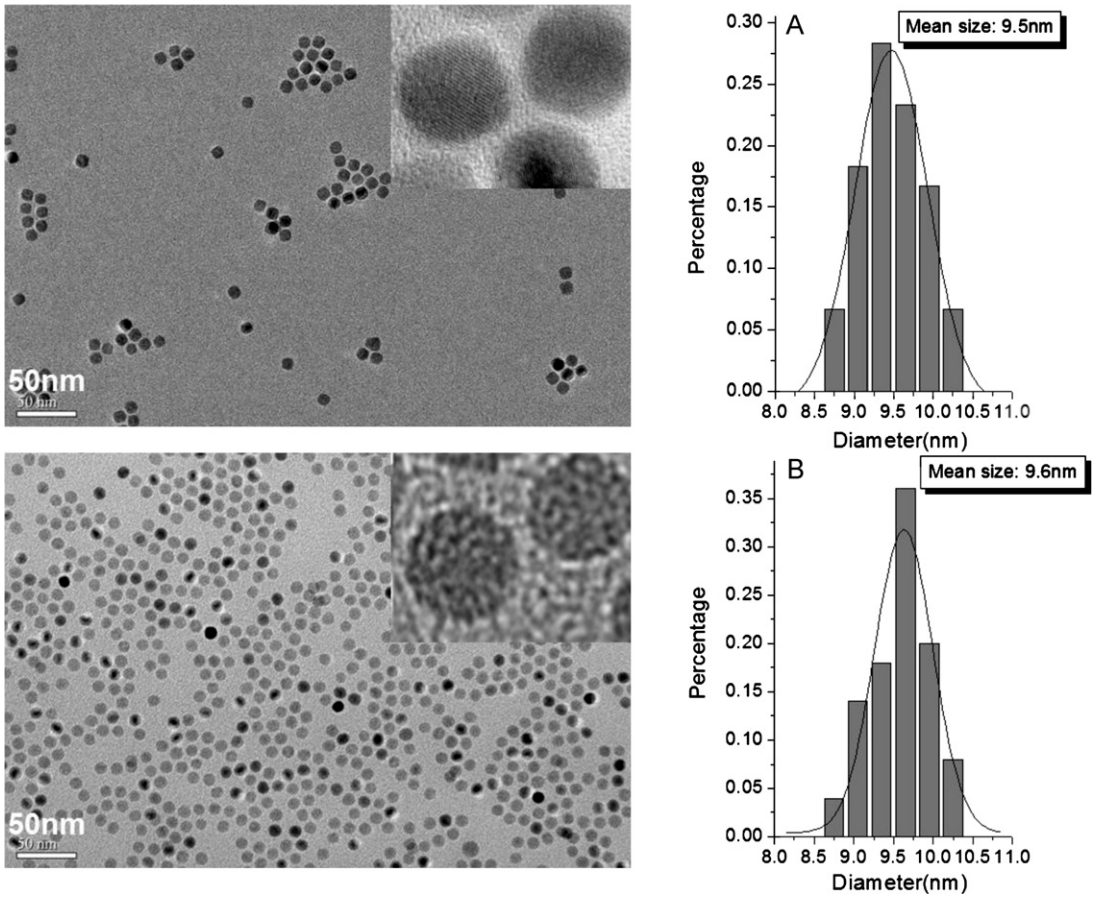

Fig. 1. TEM images of (a) quasi-cubical and (b) spherical Fe_3O_4@OA samples and their relevant size distribution histograms. Their average diameters were 9.5 nm and 9.6 nm, respectively.

of DMSA, resulting thus in the good water dispersity. It's noteworthy that this surface modification method would destroy the morphology of nanoparticles more or less [32,33]. For the quasi-cubical sample, as can be seen from the TEM images in Fig. 2a, after 30 min ligand exchange, a small part of nanoparticles changed to spherical. When the reaction time prolonged to 4 h (Fig. 2c), most nanoparticles turned spherical. Owing to their lower surface energy than quasi-cubical nanoparticles, the shape change was not obvious for the spherical samples (Fig. 2b and d). Fig. 2e and f were their high resolution TEM images of samples illustrated in Fig. 2a and b, respectively, in which the characteristic ⟨3 1 1⟩ face (fringe space = 0.25 nm) of Fe_3O_4 NPs were obvious. After surface ligand exchange reaction, all samples maintained similar diameter, as their size distribution results revealed (Fig. 2A–D). However, due to the shape change from cubical to spherical particles, the volume variation was apparent.

With energy dispersive spectrum (SEM–EDS), the element analysis regarding Fe and S was performed to quantify the DMSA on the Fe_3O_4 nanoparticles. S and Fe contents (W%) for each sample were measured, and S/Fe ratio (W_S/W_{Fe}) was calculated, which were listed in Table 1. As exchange reaction time extended, the S/Fe ratio slightly increased, indicating that the conjugating amount of DMSA did not rise largely although the exchange time prolonged by 8 times. That was to say, within the former 30 min, the exchange process was almost finished. Pons and coworkers [41] reported that the formation of disulfide bonds originated from the redox reaction between DMSA and iron oxide NPs, eventually resulted in the release of Fe^{2+} and thus nanoparticle dissolution. In contrast, the surface dissolution of the quasi-cubical nanoparticles was more obvious than spherical nanoparticles, as proved by above TEM observation. This could be attributed to preferential dissolution at corner and edge sites which are relatively low coordinated [42], as well as the high surface free energy of <111> plane. Due to the dissolution, the quasi-cubical nanoparticles have lower S/Fe ratio (about 1.0–1.2) than spherical nanoparticles (about 1.7).

Table 1
The weight ratio of S/Fe of Fe_3O_4@DMSA samples characterized by EDS.

	Quasi-cubical-30 min	Spherical-30 min	Quasi-cubical-4 h	Spherical-4 h
S(%)	50.865	63.160	54.367	63.367
Fe(%)	49.135	36.840	45.633	36.363
S/Fe	1.035	1.714	1.191	1.743

Hydrodynamic size was one most important assessment of nanoparticles used in biomedical applications. Only nanoparticles of small hydrodynamic size (always < 40 nm) could effectively avoid the abundant reticuloendothelial system (RES), and finally reach the expected targets. Furthermore, uniform hydrodynamic diameter is necessary for our studying on the sample-property relationship. Hydrodynamic sizes of four Fe_3O_4@DMSA samples were characterized by dynamic light scattering (DLS). Samples tested were enough diluted with deionized water to avoid multi-scattering effect. As the results listed in Table 2, sizes of all samples were about 20 nm, larger than the TEM size. This size increase was due to the presence of surface modified molecules and their hydration layer on the surface of nanoparticles. The uniform and ultrasmall hydrodynamic size also showed the Fe_3O_4@DMSA nanoparticles obtained by 30 min surface exchange were stable.

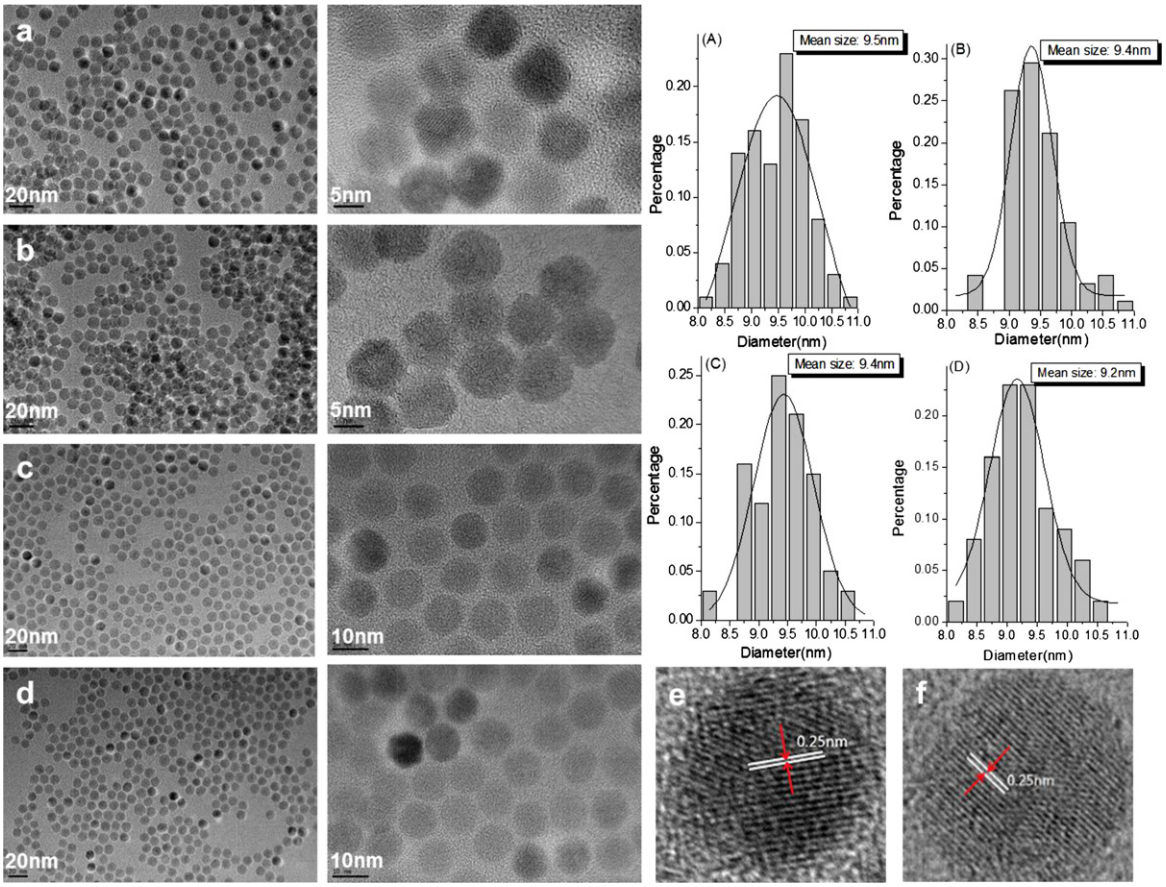

Fig. 2. TEM (a)–(d) and HRTEM (e, f) images of Fe_3O_4@DMSA samples and their respective size distribution histograms (A)–(D) (a, e) q-cubical-30 min; (b, f) spherical-30 min; (c) q-cubical-4 h; (d) spherical-4 h.

After all these elementary characterizations, we mainly focused on the magnetic properties of these Fe_3O_4@DMSA samples, and studied their morphology and surface exchange reaction time dependence.

With vibration sample magnetometer (VSM), their magnetization behavior was characterized. To more directly express their magnetism when used, samples dispersed in water were taken as subjects. UV–vis spectrophotometer was used to determine their Fe contents. Under the same Fe content, their magnetic responses were measured. From their respective hysteresis loops (Fig. 3), we could see all samples were superparamagnetic with no remanence, but with different saturation magnetization (M_s). As the exchange time prolonged from 30 min to 4 h, the saturation magnetization decreased from 48.5 emu/g to 39.0 emu/g (or 42.6 emu/g to 32.4 emu/g) for quasi-cubical samples (or spherical ones). This was due to their varied shape and surface (as the results shown in Fig. 2) and according change in core magnetic moment and surface spin canting effect [43,44]. Besides, enhanced oxidation of the surface Fe^{2+} to Fe^{3+} under longer exposure time might also account for the weakening of the magnetism. This deduction could find evidence in the comparison of Fig. 5b and c, though of similar size and shape, quasi-cubical-4 h (9.4 nm, almost spherical, Fig. 5c) had lower saturation magnetization than spherical-30 min (9.4 nm, spherical, Fig. 5b). Under the same reaction time, quasi-cubical ones had bigger saturation magnetization (48.5 emu/g > 42.6 emu/g for 30 min; 39.0 emu/g > 32.4 emu/g for 4 h) than the spherical ones, which was due to bigger magnetic core volume, as well as higher crystallinity [45] of their former lipophilic samples.

The MRI contrast enhancements also were compared for four Fe_3O_4@DMSA samples, with the results illustrated in Fig. 4. On the right, there were their respective T_2-weighted images. From top to down, with Fe concentration increasing from 0 to 10.0 μg/ml, T_2-weighted images became darker, showing enhanced negative

Table 2
Hydrodynamic sizes of four Fe_3O_4@DMSA samples in deionized water.

Hydrodynamic size (nm)			
Quasi-cubical-30 min	Spherical-30 min	Quasi-cubical-4 h	Spherical-4 h
20.42	20.30	19.37	19.44

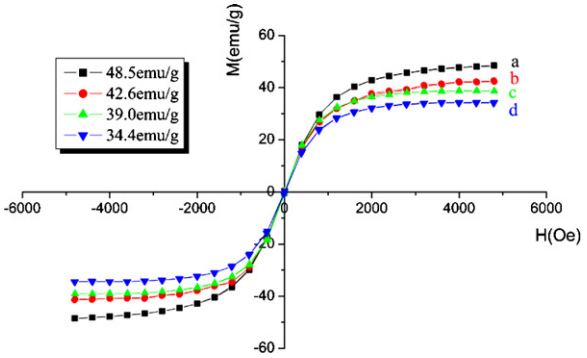

Fig. 3. Hysteresis loops of Fe_3O_4@DMSA samples.Samples tested were of identical concentration of 0.6 mg [Fe]/ml, and the results were obtained through converting the unit to emu/g. (a) quasi-cubical-30 min; (b) spherical-30 min; (c) quasi-cubical-4 h; (d) spherical-4 h.

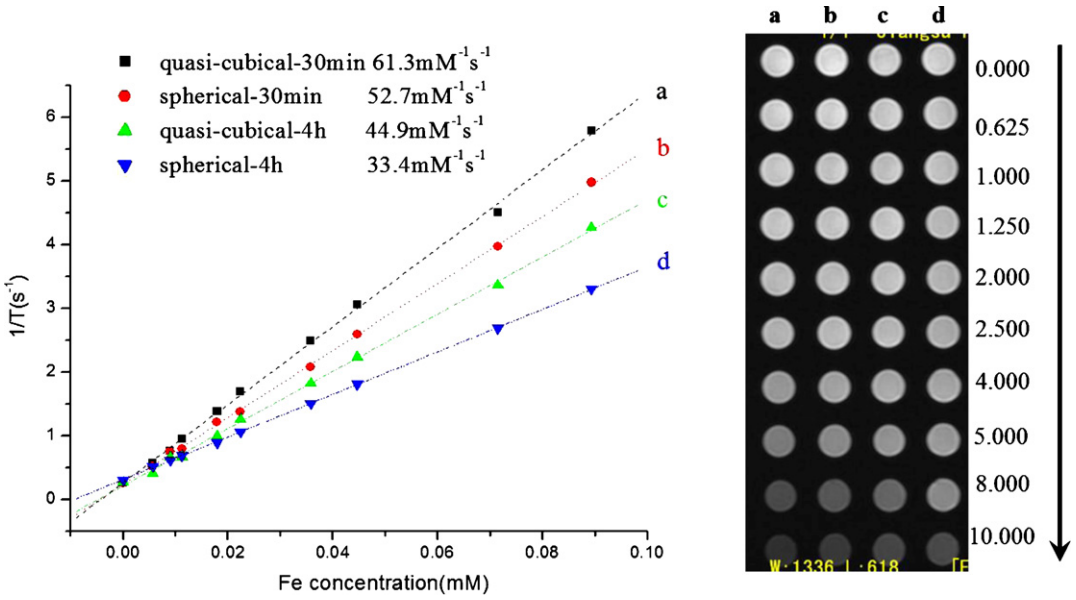

Fig. 4. T_2-weighted images of Fe_3O_4@DMSA samples in MR experiment and their relaxivities obtained with linear fitting (inverse of the relaxation times as a function of the iron concentration).

contrast effect. For each sample, a curve of $1/T_2$ versus Fe concentration was plotted. The slopes obtained through linear fit were just their transverse relaxivities (r_2). It has been demonstrated that apart from magnetic nanoparticle itself, its coatings and aggregation state are also factors influencing the relaxivity. Since all samples were coated with small DMSA molecules, and had extremely close hydrodynamic diameter, the effect of coating and aggregation could be considered to be negligible for all samples. That was to say, the difference in relaxivity should be mainly attributed to magnetic Fe_3O_4 cores and surface spin. Just as the spin–spin relaxation equation described [46]:

$$R_2 = \frac{1}{T_2} = \frac{a}{d_{NP}D}\gamma^2 m^2 C_{NP} J(\omega, \tau_D) \quad (2)$$

where a is a constant, d_{NP} the diameter of the nanoparticle, D the diffusion coefficient, m the magnetic moment of the nanoparticles, γ the gyromagnetic ratio of the water proton, C_{NP} the concentration of the nanoparticles, and $J(\omega, \tau_D)$ the spectral density function. The magnetic moment m determined the relaxivity when with same other conditions. In other words, the relaxivity depended on the magnetization of Fe_3O_4 nanoparticles. As the results shown in Fig. 4, all samples' relaxivities had the similar regularity with the VSM results.

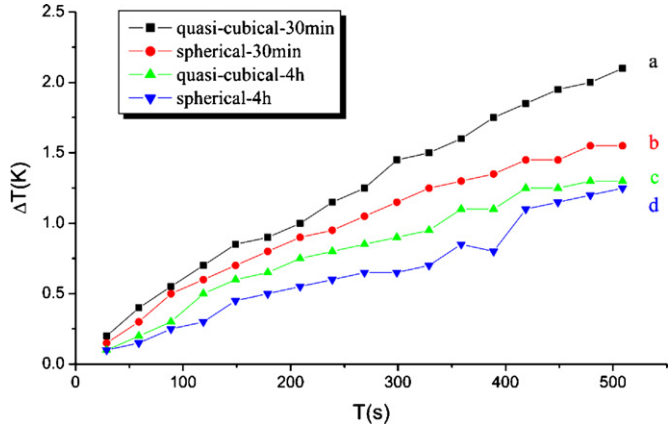

Fig. 5. Time–temperature curves for Fe_3O_4@DMSA samples under alternating magnetic field (samples were measured in aqueous phase with the concentration of 0.5 mg [Fe]/ml).

Superparamagnetic Fe_3O_4 nanoparticles can be easily magnetized as their moment paralleled with external magnetic field. Abrupt and continuous alternation of alternating current magnetic field orientation makes frictions inter- and intra-nanoparticles, and consequently the electromagnetic energy was converted into heat. This effect is attributed to Neel and Brown relaxations. And the power loss during this process is approximately given by the following equation [35]:

$$P = \frac{(mH\omega\tau)^2}{[2\tau kT\rho V(1+\omega^2\tau^2)]} \quad (3)$$

in which, m is the magnetic moment of nanoparticles, H the field amplitude, ω the measurement angular frequency, τ the relaxation time, k the Boltzmann's constant, ρ the density of magnetic nanoparticles, V the volume of nanoparticles. Under the same alternating current magnetic field, for magnetic samples of same concentration and volume, the heat converted, or the power loss depends on their respective magnetic moments. As revealed in Fig. 5, four temperature rising curves showed consistent results with the magnetism characterizations above. For the spherical-4 h sample, there was fluctuation existing due to the small Fe concentration and its relative low heat conversion capacity. Four $\Delta T/\Delta t$ values were obtained by linear fitting and substituted into equation (1) elaborated in the experimental section. Their respective SAR values were calculated, as data listed in Table 3. The quas-cubical-30 min sample had the biggest SAR value, 35.1 W/g.

All characterizations above were focused on the magnetic properties of four Fe_3O_4@DMSA samples, from which the relationship was established as followed: quasi-cubical-30 min > spherical-30 min > quasi-cubical-4 h > spherical-4 h. This can be interpreted as the following two items: First, long time exchange made the

Table 3
SAR values for the four Fe_3O_4@DMSA samples.

	Quasi-cubical-30 min	Spherical-30 min	Quasi-cubical-4 h	Spherical-4 h
$\Delta T/\Delta t$	0.00420	0.00347	0.00286	0.00209
SAR (W/g)	35.1	29.0	23.9	17.5

magnetism decreased (quasi-cubical-30 min > quasi-cubical-4 h; spherical-30 min > spherical-4 h). According to our analysis, shrinking size, damaged surface and enhanced oxidation of the samples induced by longer exchange time are all responsible. Second, quasi-cubical samples had better magnetism than spherical ones at identical condition (quasi-cubical-30 min > spherical-30 min; quasi-cubical-4 h > spherical-4 h). This is mainly arising from bigger magnetic core volume of quasi-cubical samples when of same size, and higher crystallinity might be an additional reason.

4. Conclusion

Two Monodisperse Fe_3O_4@OA nanoparticles of different shape were prepared with the thermal decomposition of iron–oleate complex. Through ligand exchange reaction, DMSA molecules modified Fe_3O_4 nanoparticles were obtained with ultrasmall hydrodynamic size and good water solubility. Our study revealed that the longer reaction time did not effectively increase the ligand exchange degree. The introduction of DMSA onto the surface promoted the Fe_3O_4 NPs dissolution, which resulted in the shape change and subsequent magnetism decline. Take their inherent magnetism as examples, comparisons between four Fe_3O_4@DMSA samples were conducted in magnetization, MRI relaxivity, and heat conversion capacity. The results showed that size, shape, crystallinity, as well as the degree of oxidation of nanoparticles determined the eventual magnetism. Bigger magnetic core volume and well crystallinity made the quasi-cubical Fe_3O_4 NPs higher magnetic performance than spherical ones of similar condition.

Acknowledgements

The work was supported by the National Important Science Research Program of China (No. 2011CB933503), National Natural Science Foundation of China (Nos. 30870679, 30970787, 31170959), and the Basic Research Program of Jiangsu Province (Natural Science Foundation, Nos. BK2011036, BK2009013).

References

[1] S. Sun, C.B. Murray, A. Moser, et al., Monodisperse FePt nanoparticles and ferromagnetic FePt nancrystals superlattices, Science 287 (2000) 1989–1992.
[2] J. Kim, J.E. Lee, T. Hyeon, et al., Generalized fabrication of multifunctional nanoparticle assemblies on silica spheres, Angew. Chem. 118 (2006) 4907–4911.
[3] S. Neveu, A. Bee, D. Talbot, et al., Size-selective chemical synthesis of tartrate stabilized cobalt ferrite ionic magnetic fluid, J. Colloid. Interface. Sci. 255 (2002) 293–298.
[4] M. Mahmoudi, A.S. Milani, P. Stroeve, Synthesis, surface architecture and biological response of superparamagnetic iron oxide nanoparticles for application in drug delivery: a review, Int. J. Biomed. Nanosci. Nanotechnol. 1 (2010) 164–201.
[5] R. Kas, E. Sevinc, U. Topal, et al., A universal method for the preparation of magnetic and luminescent hybrid nanoparticles, J. Phys. Chem. C 114 (2010) 7758–7766.
[6] A.R. Herdt, B.S. Kim, T.A. Taton, Encapsulated magnetic nanoparticles as supports for proteins and recyclable biocatalysts, Bioconjugate Chem. 18 (2007) 183–189.
[7] M. Mahmoudi, A. Simchi, A.S. Milani, et al., Cell toxicity of superparamagnetic iron oxide nanoparticles, J. Colloid. Interface Sci. 336 (2009) 510–518.
[8] A. Jordan, R. Scholz, P. Wust, et al., Magnetic fluid hyperthermia (MFH): Cancer treatment with AC magnetic field induced excitation of biocompatible superparamagnetic nanoparticles, J. Magn. Magn. Mater. 201 (1999) 413–419.
[9] A. Petri-Fink, M. Chastellain, L. Juillerat-Jeanneret, et al., Development of functionalized superparamagnetic iron oxide nanoparticles for interaction with human cancer cells, Biomaterials 26 (2005) 2685–2694.
[10] I. Hilger, R. Hergt, W.A. Kaiser, Towards breast cancer treatment by magnetic heating, J. Magn. Magn. Mater. 293 (2005) 314–319.
[11] E.V. Shevchenko, D.V. Talapin, H. Weller, et al., Colloidal synthesis and self-assembly of CoPt3 nanocrystals, J. Am. Chem. Soc. 124 (2002) 11480–11485.
[12] F. Grasset, N. Labhsetwar, J. Etourneau, et al., Synthesis and magnetic characterization of zinc ferrite nanoparticles with different environments: powder, colloidal solution, and zinc ferrite-silica core-shell nanoparticles, Langmuir 18 (2002) 8209–8216.
[13] S.J. Park, S. Kim, T. Hyeon, et al., Sythesis and magnetic studies of uniform iron nanorods and nanospheres, J. Am. Chem. Soc. 122 (2000) 8581–8582.
[14] C. Liu, B.S. Zou, Z.J. Zhang, et al., Reverse micelle synthesis and characterization of superparamagnetic $MnFe_2O_4$ spinel ferrite nanocrystallites, J. Phys. Chem. B 104 (2000) 1141–1145.
[15] J.H. Lee, Y.M. Huh, Y.W. Jun, et al., Artificially engineered magnetic nanoparticles for ultrasensitive molecular imaging, Nat. Med. 13 (2006) 95–99.
[16] E.C. Theil, Ferritin At the crossroads of iron and oxygen metabolism, J. Nutr. 133 (2003) 1549–1553.
[17] Y.W. Jun, Y.M. Huh, J. Cheon, et al., Nanoscale size effect of magnetic nanocrystals and their utilization for cancer diagnosis via magnetic resonance imaging, J. Am. Chem. Soc. 127 (2005) 5732–5733.
[18] H.W. Duan, M. Kuang, S.M. Nie, et al., Reexamining the effects of particle size and surface chemistry on the magnetic properties of iron oxide nanocrystals: New insights into spin disorder and proton relaxivity, J. Phys. Chem. C. 112 (2008) 8127–8131.
[19] U.I. Tromsdorf, N.C. Bigall, H. Weller, et al., Size and surface effects on the MRI relaxivity of manganese ferrite nanoparticle contrast agents, Nano Letters. 7 (2007) 2422–2427.
[20] H.B. Na, I.C. Song, T. Hyeon, Inorganic nanoparticles for MRI contrat agents, Adv. Mater. 21 (2009) 2133–2148.
[21] R. Hergt, R. Hiergeist, U. Richter, et al., Maghemite nanoparticles with very high AC-losses for application in RF-magnetic hyperthermia, J. Magn. Magn. Mater. 270 (2004) 345–357.
[22] J.P. Fortin, C. Wilhelm, F. Gazeau, et al., Size-sorted anionic iron oxide nanomagnets as colloidal mediators for magnetic hyperthermia, J. Am. Chem. Soc. 129 (9) (2007) 2628–2635.
[23] Y.W. Jun, J.H. Lee, J. Cheon, Chemical design of nanoparticle probe for high-performance magnetic resonance, Angew. Chem. Int. Ed. 47 (2008) 5122–5135.
[24] Y.Q. Ge, Y. Zhang, N. Gu, et al., Effect of surface charge and agglomerate degree of magnetic iron nanoparticles on KB cellular uptake in vitro, Colloid. Surface B 73 (2009) 294–301.
[25] A.G. Roca, S.V. Verdaguer, M.P. Morales, et al., Effect of nanoparticle and aggregate size on the relaxometric properties of MR Contrast agents based on high quality magnetite nanopartilces, J. Phys. Chem. B 113 (2009) 7033–7039.
[26] G. Salazar-Alvarez, J. Qin, J. Nogues, et al., Cubic versus spherical magnetic nanoparticles: the role of surface anisotropy, J. Am. Chem. Soc. 130 (2008) 13234–13239.
[27] S. Sun, H. Zeng, Size-controlled synthesis of magnetite nanoparticles, J. Am. Chem. Soc. 124 (2002) 8204–8205.
[28] S. Sun, H. Zeng, D.B. Robinson, et al., Monodisperse MFe2O4 (M = Fe, Co, Mn) nanoparticles, J. Am. Chem. Soc. 126 (2004) 273–279.
[29] N.R. Jana, Y. Chen, X.G. Peng, Size- and shape-controlled magnetic (Cr, Mn, Fe, Co, Ni) oxide nanocrystals via a simple and general approach, Chem. Mater. 16 (2004) 3931–3935.
[30] J. Park, K. An, T. Hyeon, et al., Ultra-large-scale syntheses of monodisperse nanocrystals, Nat. Mater. 3 (2004) 891–895.
[31] Z.P. Chen, Y. Zhang, N. Gu, et al., Preparation and characterization of water-soluble monodisperse magnetic iron oxide nanoparticles via surface double-exchange with DMSA, Colloid. Surf. A 316 (2008) 210–216.
[32] J. Aldana, N. Lavelle, X. Peng, et al., Size-dependent dissociation pH of thiolate ligands from cadmium chalcogenide nanocrystals, J. Am. Chem. Soc. 127 (2005) 2496–2504.
[33] S.K. Basiruddin, A. Saha, N.R. Jana, et al., Advances in coating chemistry in deriving soluble functional nanoparticle, J. Phys. Chem. C 114 (2010) 11009–11017.
[34] A.E. Harvey, J.A. Smart, E.S. Amis, et al., Simultaneous spectrophotometric determination of iron(II) and total iron with 1,10-phenanthroline, Anal. Chem. 27 (1955) 26–29.
[35] M. Ma, Y. Wu, N. Gu, et al., Size dependence of specific power absorption of Fe3O4 particles in AC magnetic field, J. Magn. Magn. Mater. 268 (2004) 33–39.
[36] J.L. Campbell, J. Arora, V. Bansal, et al., Quasi-cubic magnetite/sililca core-shell nanoparticles as enhanced MRI contrast agents for cancer imaging, Plos One 7 (2011) 1–8.
[37] J. Park, J. Joo, T. Hyeon, Synthesis of monodisperse spherical nanocrystals, Angew. Chem. Int. Ed. 46 (2007) 4630–4660.
[38] C.M. Fang, S.C. Parker, G. De With, Atomistic simulation of the surface energy of spinel $MgAl_2O_4$, J. Am. Chem. Soc. 83 (2000) 2082.
[39] N.Z. Bao, L.M. Shen, A. Gupta, et al., Formation mechanism and shape control of monodisperse magnetic $CoFe_2O_4$ nanocrystals, Chem. Mater. 21 (2009) 3458–3468.
[40] M.V. Kovalenko, M.I. Bodnarchuk, R.T. Lechner, et al., Fatty acid salts as stabilizers in size- and shape-controlled nanocrystal synthesis: the case of inverse spinel iron oxide, J. Am. Chem. Soc. 129 (2007) 6352–6353.
[41] N. Fauconnier, J.N. Pons, A. Bee, et al., Thiolation of maghemite nanoparticles by dimercaptosuccinic acid, Colloid. Surf. A 194 (1997) 427–433.
[42] Q. Hua, W.X. Huang, Chemical etching induced shape change of magnetite microcrystals, J. Mater. Chem. 18 (2008) 4286–4290.

[43] M.P. Morales, M. Andres-Verges, S. Veintemillas-Verdaguer., Structural effects on the magnetic properties of γ-Fe_2O_3 nanoparticles, J. Magn. Magn. Mater. 203 (1999) 146–148.
[44] M.P. Morales, S. Veintemillas-Verdaguer, C.J. Serna, Surface and internal spin canting in γ-Fe_2O_3 nanoparticles, Chem. Mater. 11 (1999) 3058–3064.
[45] L. Zhen, S. Qiao, M.Y. Gao, Preparation of water-soluble magnetite nanocrystals from hydrated ferric salts in 2-pyrrolidone: mechanism leading to Fe_3O_4, Angew. Chem. Int. Ed. 44 (2005) 123–126.
[46] H.B. Na, I.C. Song, T. Hyeon, Inorganic nanoparticles for MRI contrast agents, Adv. Mater. 21 (2009) 2133–2148.